SPECIAL DIMES COLLECTION

Vertical Flow in the Southern Ocean Estimated from Individual Moorings

F. SÉVELLEC, A. C. NAVEIRA GARABATO, J. A. BREARLEY,* AND K. L. SHEEN

Ocean and Earth Science, National Oceanography Centre Southampton, University of Southampton, Southampton, United Kingdom

(Manuscript received 14 February 2014, in final form 26 March 2015)

ABSTRACT

This study demonstrates that oceanic vertical velocities can be estimated from individual mooring measurements, even for nonstationary flow. This result is obtained under three assumptions: (i) weak diffusion (Péclet number $\gg 1$), (ii) weak friction (Reynolds number $\gg 1$), and (iii) small inertial terms (Rossby number $\ll 1$). The theoretical framework is applied to a set of four moorings located in the Southern Ocean. For this site, the diagnosed vertical velocities are highly variable in time, their standard deviation being one to two orders of magnitude greater than their mean. The time-averaged vertical velocities are demonstrated to be largely induced by geostrophic flow and can be estimated from the time-averaged density and horizontal velocities. This suggests that local time-mean vertical velocities are primarily forced by the time-mean ocean dynamics, rather than by, for example, transient eddies or internal waves. It is also shown that, in the context of these four moorings, the time-mean vertical flow is consistent with stratified Taylor column dynamics in the presence of a topographic obstacle.

1. Introduction

Oceanic vertical flow is an important element of the ocean circulation, playing a central role in the redistribution of water and tracers between (and within) the upper-ocean mixed layer and the ocean interior. In the interior, the occurrence of vertical motion is associated with a wide range of processes characterized by distinct dynamics: from relatively high-frequency and small-scale geostrophically unbalanced flows (such as internal waves and three-dimensional turbulent motions; e.g., Polzin et al. 1997; D'Asaro et al. 2007; Waterman et al. 2013; Sheen et al. 2013) to near-bottom frictional Ekman currents along sloping topographic boundaries (Garrett et al. 1993), wind-driven Ekman motions, and rectified mesoscale eddy flows along sloping isopycnals (Marshall and Speer 2012, and references therein). The latter two mechanisms are believed to extensively underpin vertical flow in the Southern Ocean, a region hosting a prominent large-scale vertical circulation of global significance (Rintoul and Naveira Garabato 2013). This view of the Southern Ocean stems from simple theoretical models of the regional circulation (Olbers et al. 2004) and is found to hold in general circulation models of varying degrees of idealization and eddy-permitting capability (Abernathey et al. 2011; Hallberg and Gnanadesikan 2006; Farneti and Delworth 2010). Nonetheless, the weakness and wide spatial distribution of the vertical flows associated with these processes have to date impeded their assessment from observations.

Historically, the computation of vertical velocities has been done using the well-known omega equation (Holton 1972). This equation relates the vertical motion to measurable features (density, temperature, pressure, and horizontal flows) and is derived from a combination of the continuity, thermodynamic, and

Denotes Open Access content.

* Current affiliation: British Antarctic Survey, Cambridge, United Kingdom.

Corresponding author address: F. Sévellec, Ocean and Earth Science, University of Southampton, Waterfront campus, European Way, Southampton, SO14 3ZH, United Kingdom.
E-mail: florian.sevellec@noc.soton.ac.uk

DOI: 10.1175/JPO-D-14-0065.1

momentum equations. The omega equation has the advantage of being a diagnostic (i.e., no time derivative) of the state of the system, so that a single snapshot is enough to determine the vertical flow. However, the equation requires a fine spatial discretization (i.e., spatial derivatives along the three spatial dimensions). It has been shown to be extremely useful in the atmosphere, where radiosondes capture accurately the three-dimensional system's state on a global scale at a given instant (but repeated measurements at the same location are impossible, that is, time derivatives are not measurable). In the ocean, spatial sampling is much sparser, making implementation of this equation difficult. However, oceanographic moorings, which measure the ocean at a single location but with high temporal resolution, allow an alternative approach to be adopted. Here, we derive a new equation based on a combination of the momentum and thermodynamic equations, which utilizes the time evolution of the local horizontal velocity and density field to provide robust estimates of vertical velocity.

In this study, we characterize the vertical motion in a 10.5 km × 10.5 km patch of the Southern Ocean and investigate its underpinning physics using measurements from a cluster of moorings deployed in Drake Passage as part of the Diapycnal and Isopycnal Mixing Experiment in the Southern Ocean (DIMES). Time series of vertical velocity profiles are estimated from individual moorings by deriving and applying an expression for the vertical flow in terms of the temporal and vertical variations of density and horizontal velocity, generalized from the work of Bryden (1980) to include ageostrophic and time-varying forcings. We show that, in this area, time-mean vertical motion in the deep ocean is primarily determined by the properties of the time-mean horizontal flow, which exhibits a spatial structure consistent with the occurrence of a stratified Taylor column over a topographic obstacle encompassed by the moorings. Unlike in classical Taylor column theory for a uniform fluid, which induces a vertically uniform horizontal deviation in the presence of a topographic obstacle to conserve potential vorticity, with stratification the Taylor column is restricted to the deep ocean. Because stratification restricts the horizontal deviation to the vicinity of the topographic obstacle, there is a change in the horizontal flow orientation with depth. In accordance with Bryden (1980), a steady vertical flow must occur in association with this change in order to conserve density. Here, we will demonstrate that, following stratified Taylor column dynamics, a vertical flow occurs above the topographic obstacle encompassed by the moorings.

The paper is organized as follows: In section 2, we derive the expression used to estimate the vertical velocity from individual mooring measurements. The data and analytical methodology are introduced in section 3. Section 4 describes the results of our analysis. The main findings of this work are synthesized in section 5.

2. Theory

In this section, we use the thermodynamic equation for the advection of density to calculate the vertical velocity.[1] The set of equations (in Cartesian coordinates) from which our results are derived are given below. These encompass the horizontal momentum equations, hydrostatic balance, nondivergence (i.e., the Boussinesq approximation), and the evolution of density forced by advective and diffusive processes:

$$D_t u - fv = -\frac{1}{\rho_0}\partial_x P + \text{Visc}, \tag{1a}$$

$$D_t v + fu = -\frac{1}{\rho_0}\partial_y P + \text{Visc}, \tag{1b}$$

$$\partial_z P = -\rho g, \tag{1c}$$

$$\partial_x u + \partial_y v + \partial_z w = 0, \quad \text{and} \tag{1d}$$

$$D_t \rho = \text{Diff}. \tag{1e}$$

Here, t is time; x, y, and z are the zonal, meridional, and vertical coordinates; u, v, and w are the zonal, meridional, and vertical velocities; P is the pressure; ρ (ρ_0) is the (reference) density; f is the Coriolis parameter; g is Earth's gravity acceleration; ∂_t, ∂_x, ∂_y, and ∂_z are the time, zonal, meridional, and vertical partial derivatives; D_t is the material derivative ($=\partial_t + u\partial_x + v\partial_y + w\partial_z$); and Visc and Diff are viscosity and diffusivity operators, respectively.

We simplify this set of equations further by assuming low viscosity (Re $\gg$ 1, Visc is negligible), small inertial terms (Ro $\ll$ 1, advective terms are negligible in the horizontal momentum equations), and low diffusion (Pe $\gg$ 1, Diff is negligible). The quantity Re is the Reynolds number and measures the ratio of inertial to viscous forces; Ro is the Rossby number and measures the ratio of inertial forces to the Coriolis acceleration; and Pe is the Péclet number and measures the ratio of advective to diffusive terms. (An estimation of the vertical Rossby number can be found in section 5.) Applying these assumptions, the set in (1) reduces to

[1] Two other methods exist to calculate the vertical velocity but are inconsistent with the available dataset. One possible approach would entail the derivation of vertical velocity from the divergence of the horizontal velocity field. However, the spatial derivatives involved cannot be estimated accurately by using neighboring moorings (since these may be too far apart to resolve the scales of the key processes involved). The other alternative would be to combine the momentum and continuity equations, yet this would lead to an even more complex expression with more unknowns (i.e., the equation of vorticity conservation in its quasigeostrophic form).

TABLE 1. Current meter and moored CTD nominal depths for the DIMES C mooring and the four corner moorings (SW, SE, NE, and NW). Data were returned between 12 Dec 2009 and 6 Dec 2010 and between 20 Dec 2010 and 5 Mar 2012. The exact instrument depths vary slightly between the four corner moorings because of subtle differences in mooring design. Both the SW and NE moorings suffered from a buoyancy implosion early in the first year of deployment, such that they only recorded ~45 days of data in that year. Other early instrument failures occurred during the first deployment of the SE mooring. Owing to these issues, we exclude first-year data from the analysis of the SW, NE, and SE moorings. Full details of the instruments used in each year can be found in the cruise reports (Naveira Garabato 2010; Meredith 2011).

Location	Instrument type	Nominal depths (m)
C mooring	Nortek acoustic current meter	425, 475, 525, 575, 1200, 1299, 1853, 1951, 2049, 2152, 3400, 3600
	Seabird MicroCAT [serial interface, memory, and integral pump (SMP)]	425, 475, 525, 575, 1200, 1299, 1853, 1951, 2049, 2152, 3400, 3600
NW, SW, NE, and SE moorings	Seaguard/Sontek/Nortek acoustic current meter	450, 550, 1250, 2000, 3400
	Seabird MicroCAT [SMP/inductive modem and integral pump (IMP)]	450, 550, 1250, 2000, 3400

$$\partial_t u - fv = -\frac{1}{\rho_0}\partial_x P, \tag{2a}$$

$$\partial_t v + fu = -\frac{1}{\rho_0}\partial_y P, \tag{2b}$$

$$\partial_z P = -\rho g, \quad \text{and} \tag{2c}$$

$$D_t \rho = 0. \tag{2d}$$

The set in (2) is compatible with quasigeostrophic dynamics, which appear as the next order balance (Pedlosky 1979) where the evolution of relative vorticity ($\zeta = \partial_x v - \partial_y u$) may be obtained by retaining the $O(\mathrm{Ro})$ correction in (1a), (1b), and (1d). This group of equations can be applied to flows characterized by a horizontal scale larger than the Rossby deformation radius (Pedlosky 1979). Further, by retaining the acceleration term in the horizontal momentum equations, we capture the effects of a class of higher-frequency flows (e.g., internal waves and tides) that are not considered in quasigeostrophic dynamics. However, this set of equations neglects the advection term in the momentum balance, which is important for turbulent density currents (Manucharyan et al. 2014), Kelvin–Helmholtz instability (Cushman-Roisin and Beckers 2011), and internal solitons (Osborne and Burch 1980), for instance.

Applying hydrostatic balance to the two momentum equations in (2) and expanding the material derivative in the density equation, we obtain

$$\frac{g}{\rho_0}\partial_x \rho = \partial_t \partial_z u - f\partial_z v, \tag{3a}$$

$$\frac{g}{\rho_0}\partial_y \rho = \partial_t \partial_z v + f\partial_z u, \quad \text{and} \tag{3b}$$

$$w\partial_z \rho = -\partial_t \rho - u\partial_x \rho - v\partial_y \rho. \tag{3c}$$

Assuming stable stratification [i.e., $N^2 = -(g/\rho_0)\partial_z \rho > 0$, where N is the Brunt–Väisälä frequency] yields

$$w = -\frac{\partial_t \rho}{\partial_z \rho} + \frac{f}{N^2}(v\partial_z u - u\partial_z v) + \frac{1}{N^2}(u\partial_t \partial_z u + v\partial_t \partial_z v). \tag{4}$$

Decomposing the horizontal velocity into an amplitude R and an angle ϕ (measured anticlockwise from eastward), we obtain $u = R\cos\phi$ and $v = R\sin\phi$. Substituting this notation into the right-hand side of (4), we express the term associated with geostrophic horizontal advection as $v\partial_z u - u\partial_z v = -R^2\partial_z \phi$. Equivalently, the term linked to ageostrophic horizontal advection

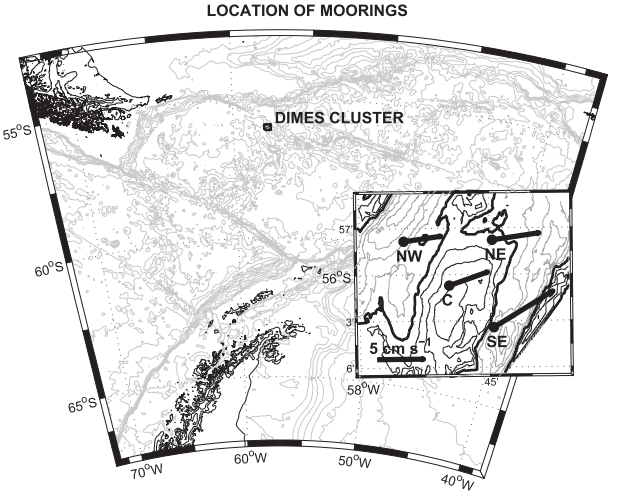

FIG. 1. Location of the DIMES mooring array. The inset shows a magnification of the region. Black circles denote the locations of the four (NW, NE, C, and SE) moorings used in this study. The thick black lines indicate the exact depth-averaged direction and intensity of the northeastward flow at the moorings' location. In the main panel, light gray contours indicate submarine topography, with a contour interval of 500 m; black contours mark coastlines. In the inset, the solid thick contours represent the 4000-m isobath, with solid black and gray contours denoting shallower and deeper isobaths at intervals of 100 m.

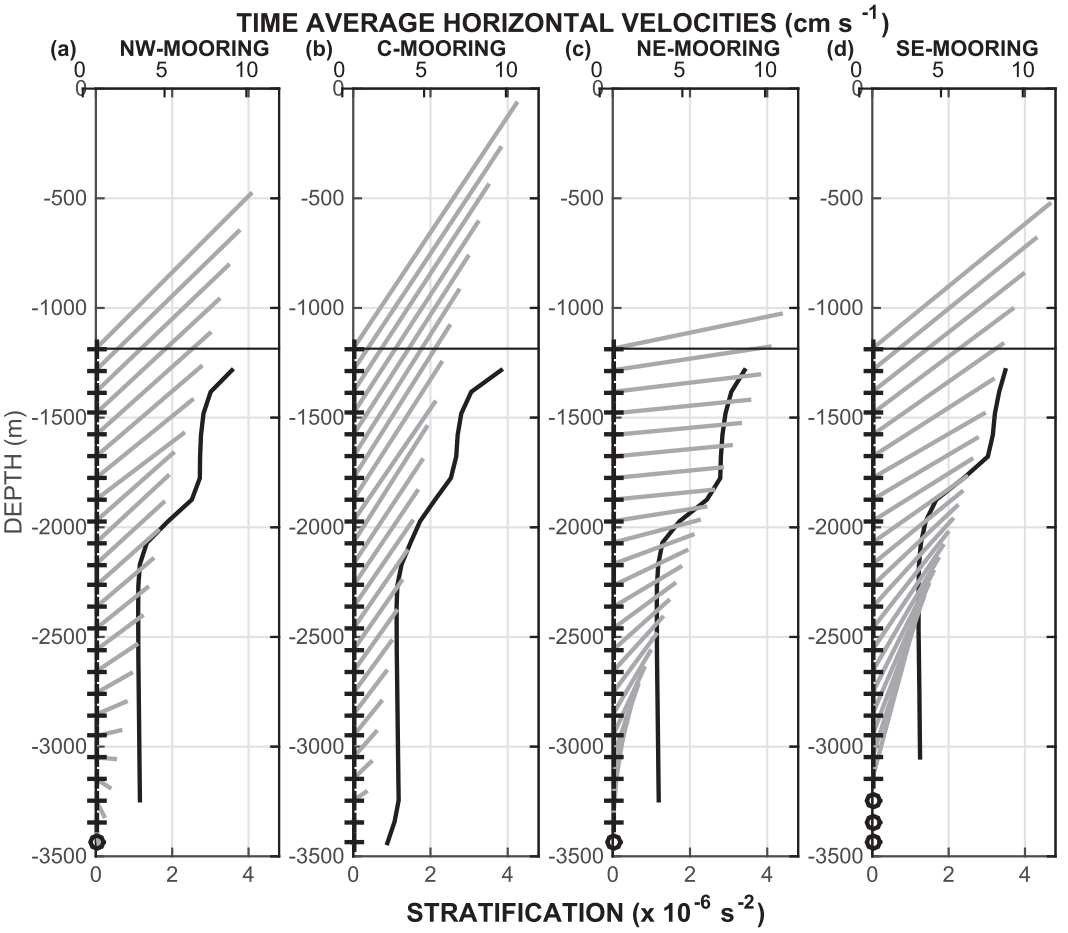

FIG. 2. Time-mean horizontal velocity and stratification for the four moorings: (a) NW, (b) C, (c) NE, and (d) SE. Thick black lines indicate the squared buoyancy frequency. Gray lines show the horizontal velocity vectors at the depth of their tail point, indicated by a cross. Vectors pointing to the right denote eastward flow, and vectors pointing upward denote northward flow. Open circles indicate water column segments where lack of data prevented the robust computation of velocity and stratification.

becomes $u\partial_t\partial_z u + v\partial_t\partial_z v = R\partial_t\partial_z R - R^2\partial_t\phi\partial_z\phi$. Vertical velocity may thus be defined as

$$w = -\frac{\partial_t\rho}{\partial_z\rho} - \frac{R^2}{N^2}(f + \partial_t\phi)\partial_z\phi + \frac{R}{N^2}\partial_t\partial_z R. \qquad (5)$$

This equation demonstrates that vertical velocity can be estimated from a time series of density and horizontal velocity measurements at multiple depth levels from a single mooring.

Asymptotically, that is, at steady state ($\partial_t \to 0$), (5) is equivalent to the classical result of Bryden (1980):

$$w_g = -f\frac{R^2}{N^2}\partial_z\phi, \qquad (6a)$$

where w_g is the vertical velocity associated with horizontal geostrophic advection.

The total vertical velocity in (5) can be decomposed into w_g and two further contributions: the vertical velocity associated with horizontal ageostrophic advection w_a, defined as

$$w_a = -\frac{R^2}{N^2}\partial_t\phi\partial_z\phi + \frac{R}{N^2}\partial_t\partial_z R, \qquad (6b)$$

and the vertical velocity linked to the unsteady behavior of density w_u, given by

$$w_u = -\frac{\partial_t\rho}{\partial_z\rho}. \qquad (6c)$$

Linearization of (6c), around a steady vertical density structure and in the absence of steady vertical flow, is often considered as an approximation of the vertical velocities induced by internal waves (Krauss 1966; Gill 1982; van Aken et al. 2007).

TABLE 2. Main characteristics of the vertical velocity from (8) for each component [w_g (GEO), w_a (AGEO), and w_u (UNS)] and the total (w), following (6). The bold font denotes the dominant value in each component.

	GEO	AGE	UNS	TOTAL
NW mooring				
μ ($\times 10^{-5}$ m s^{-1})	**7.2**	0.50	−0.13	8.1
$\lambda_{t,z}$ ($\times 10^{-5}$ m s^{-1})	**3.3**	0.21	0.45	2.9
$\lambda_{z,t}$ (mm s^{-1})	0.66	0.64	**6.2**	6.5
$\sigma_{t,z}$ (mm s^{-1})	0.83	1.2	**7.9**	8.1
$\sigma_{z,t}$ (mm s^{-1})	0.34	0.67	**4.5**	4.4
C mooring				
μ ($\times 10^{-5}$ m s^{-1})	**−3.0**	−0.45	1.0	−2.4
$\lambda_{t,z}$ ($\times 10^{-5}$ m s^{-1})	**6.4**	4.5	1.9	4.7
$\lambda_{z,t}$ (mm s^{-1})	0.63	0.78	**5.6**	5.8
$\sigma_{t,z}$ (mm s^{-1})	1.5	3.4	**8.3**	9.2
$\sigma_{z,t}$ (mm s^{-1})	1.1	3.0	**5.5**	6.5
NE mooring				
μ ($\times 10^{-5}$ m s^{-1})	**−5.1**	0.74	0.34	−4.1
$\lambda_{t,z}$ ($\times 10^{-5}$ m s^{-1})	**4.9**	0.42	0.55	4.7
$\lambda_{z,t}$ (mm s^{-1})	0.57	0.70	**6.3**	6.4
$\sigma_{t,z}$ (mm s^{-1})	0.77	1.3	**8.1**	8.2
$\sigma_{z,t}$ (mm s^{-1})	0.35	0.84	**4.5**	4.6
SE mooring				
μ ($\times 10^{-5}$ m s^{-1})	**−8.4**	0.95	0.01	−7.4
$\lambda_{t,z}$ ($\times 10^{-5}$ m s^{-1})	**12**	0.45	0.28	11
$\lambda_{z,t}$ (mm s^{-1})	0.54	0.86	**6.4**	6.5
$\sigma_{t,z}$ (mm s^{-1})	0.82	1.4	**7.9**	8.0
$\sigma_{z,t}$ (mm s^{-1})	0.38	0.77	**4.2**	4.4

Finally, it is insightful to decompose w_g into its time-dependent and time-mean components as

$$\langle w_g \rangle_t = -\frac{\langle w_g' N^{2\prime} \rangle_t}{\langle N^2 \rangle_t} - f\frac{\langle R^2 \rangle_t}{\langle N^2 \rangle_t}\partial_z \langle \phi \rangle_t - f\frac{\langle R^{2\prime}\partial_z \phi' \rangle_t}{\langle N^2 \rangle_t}, \qquad (7)$$

where $\langle X \rangle_t = \int_{t_i}^{t_f} X\, dt/T$ and X' respectively denote the time average and temporal anomaly of any variable X (such that $X' = X - \langle X \rangle_t$), with $T = t_f - t_i$ being the duration of the dataset and t_i and t_f being the initial and final times of the dataset.

3. Data and methods

a. Data

The theoretical framework introduced in the previous section is tested by applying it to measurements of horizontal velocity u, v and in situ density ρ from four moorings of the DIMES array (Brearley et al. 2013; see also Table 1 for a list of mooring instrumentation). These were deployed between 12 December 2009 and 5 March 2012 over a ~900-m-high topographic feature in northern Drake Passage (Fig. 1). The mooring array spanned an area of 10.5 km × 10.5 km and was composed of six moorings in total. Data from the NW (55°58′S, 57°56′W), C (56°S, 57°50′W), NE (55°58′S, 57°45′W), and SE (56°03′S, 57°45′W) moorings are considered here. The flow in this region is strongly time variable, is oriented northeastward when averaged over the mooring deployment period (Fig. 1), and is intensified at the surface.

Data from the M and SW moorings are not used here. Since the M mooring was only instrumented with current meters and moored CTDs at two deep levels, it lacks the vertical resolution to draw robust conclusions on the properties of vertical flow. The SW mooring was instrumented at five levels (identically to the NW, NE, and SE moorings) but yielded only 150 days of data due to a buoyancy implosion in the first year and instrumental failure in the second year of deployment. As shown in the next section, 150 days is insufficient to obtain a stable estimate of the time-mean vertical velocity; convergence only occurs after roughly 1 yr. Observations from the other moorings span 815 days. A detailed account of the quality control on the CTD and current meter data is given in Brearley et al. (2013).

Large mooring knockdowns (of up to 800 m) were experienced by all moorings because of instances of intense flow associated with Antarctic Circumpolar Current (ACC) jets and eddies. Consideration was therefore given to the issue of mooring motion correction. Most mooring motion correction schemes for velocity (e.g., Cronin et al. 1992) rely on the geostrophic approximation. This is an assumption we do not wish to make here, as one of the goals of this work is to examine the relative contributions of geostrophic and ageostrophic terms to vertical flow. We thus chose to linearly interpolate measurements of potential temperature θ, salinity S, u, and v onto surfaces of constant pressure at 100-dbar intervals and confined our analysis to the part of the water column that had measurements at all times (i.e., depths greater than 1300 m). However, we did test the sensitivity of our results by using a statistical mooring motion correction. For this purpose we created canonical (third-order polynomial) profiles for zonal and meridional velocity (u and v) and then computed velocity from the distance-weighted in situ and canonical profiles. (It should be noted that this method has a different disadvantage in that it assumes a background oceanic velocity structure.) The simple linear interpolation and the more complex statistical mooring correction lead to virtually the same results, with a maximum error of 5% in the time-mean vertical velocity estimates. In the remainder of this study, only results based on linear interpolation are shown. Density and depth were computed from temperature, salinity, and pressure using the Gibbs Seawater oceanographic toolbox (McDougall and Barker 2011) and following the gamma global polynomial for neutral density (Sérazin 2011).

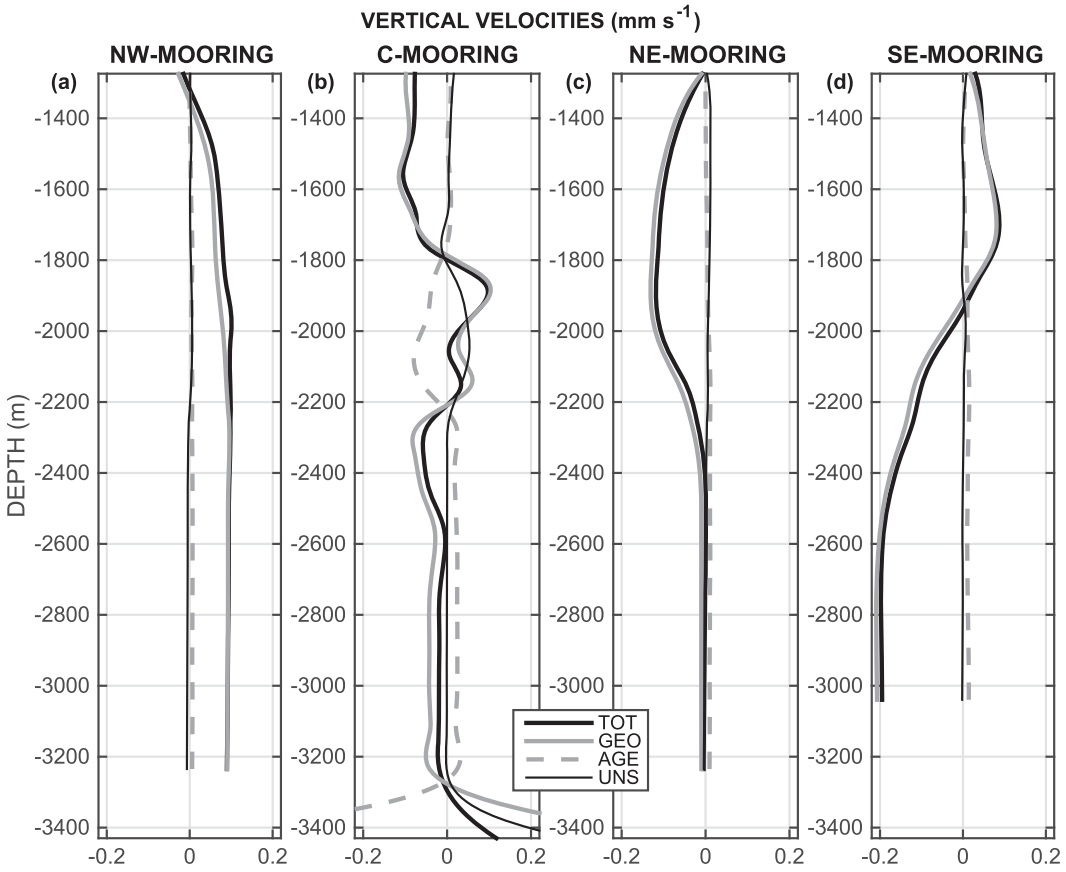

FIG. 3. Time-mean vertical velocities computed for the four moorings (a) NW, (b) C, (c) NE, and (d) SE following (5). For each mooring, w is decomposed into its three components, following (6): w_g (thick solid gray), w_a (thick dashed gray), and w_u (thin solid black). The total vertical velocity is shown in thick solid black.

To estimate the impact of the measurement uncertainty in the vertical velocity computation, we propagate the measurement uncertainty in (5), (6a), (6b), and (6c). We assume a measurement uncertainty of 4×10^{-3} K for temperature and 8×10^{-3} psu for salinity (after calibration of the moored CTDs by reference to ship-based CTD measurements). Current meter speed accuracies are given as 1% of the measured value $\pm 0.5\,\mathrm{cm\,s^{-1}}$, based on the manufacturer's specifications for Nortek and Seaguard current meters, the most commonly used instruments in the array. For example, a time and space average measured velocity speed of $12\,\mathrm{cm\,s^{-1}}$ is associated with an error of $0.1 + 0.5 = 0.6\,\mathrm{cm\,s^{-1}}$, while for the angle, it is 2° or 3×10^{-2} radians. Allowing all these errors to accumulate gives an overall error for each vertical velocity estimate of 60% for the geostrophic component, 115% for the ageostrophic component, and less than 0.3% for the unsteady component (which is related only to density). The relative error on the total vertical velocity is 68%. Although these errors seem large, it is worth emphasizing that this assumes that all errors are acting in the same direction (i.e., a worst case scenario is assumed in which θ, S, and velocity errors accumulate). Further, this study focuses on the long-term average properties of vertical velocity, with over $n \simeq 40\,000$ samples (for $T = 400$ days). Assuming a normal distribution for the errors, the total error scales as $1/\sqrt{n}$, leading to a time-mean geostrophic and ageostrophic error of 0.3% and 0.6%, respectively.

We also considered the effect of underestimation of tidal currents due to mooring knockdown (e.g., through current meters being displaced into deeper regions of weaker flows). However, these errors are small due to the dominant M_2 and S_2 tidal currents being relatively weak ($<1\,\mathrm{cm\,s^{-1}}$) and only increasing very slowly with depth in the upper part of the water column where mooring knockdown is significant.

The vertical resolution is the main limitation of the dataset. From (6a), (6b), and (6c), it may be seen that the geostrophic, ageostrophic, and unsteady components of the vertical velocity are only dependent on a first vertical derivative. Hence, vertical resolution affects each

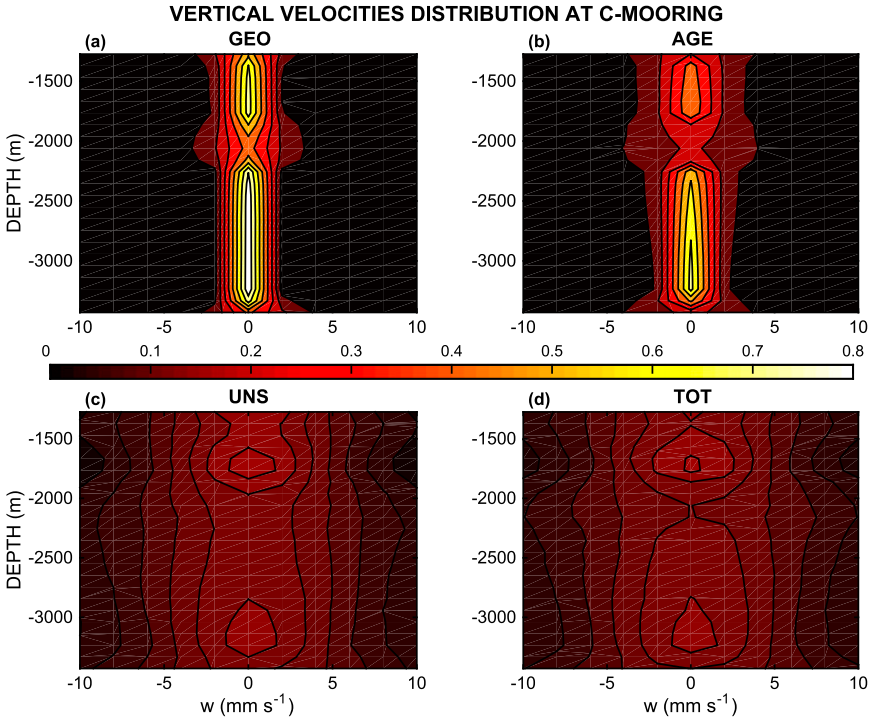

FIG. 4. Distribution of the vertical velocity at the C mooring as a function of depth: (a) w_g, (b) w_a, (c) w_u, and (d) total vertical velocity.

component in the same way: the first baroclinic mode of an inertial-gravity wave is described as well as the first baroclinic mode of a geostrophic flow, for instance. However, in the ocean we expect vertical motion for the nongeostrophic terms (e.g., an internal wave beam) on smaller vertical scales than for the geostrophic term (i.e., nongeostrophic terms often act on higher-order baroclinic mode than geostrophic term). This implies that the nongeostrophic terms are likely more affected by the relatively low vertical resolution of the dataset.

The effect of the spatial and temporal resolutions of the data on the sign and magnitude of the calculated vertical velocities was assessed by withholding data at one or more vertical levels prior to linear interpolation of the measurements. This had little qualitative impact on the results, and both the total and geostrophic components of w were largely unaffected in quantitative terms. For example, computation of vertical velocity from C mooring data degraded to only five instrumented levels (i.e., equivalent to the NW, NE, and SE moorings) led to a difference of 10% on w_g. However, w_a and w_u did change significantly (i.e., on the order of 1). For these terms, high vertical resolution is required to accurately represent the effects of internal wave motions. This is not a serious limitation, as the nongeostrophic terms are not dominant (see section 4) even when the vertical resolution of the data is modified. Thus, we have confidence in the spatiotemporal resolution of the data being sufficient to support the main conclusions of our analysis.

b. Methods

To characterize the properties of the diagnosed vertical flow, we apply a number of basic diagnostics to the total vertical velocity w or any of its three components w_g, w_a, and w_u. These are

$$\mu = \langle w \rangle_{t,z}, \tag{8a}$$

$$\lambda_{t,z} = \sqrt{\langle \langle w \rangle_t^2 \rangle_z - \langle \langle w \rangle_t \rangle_z^2}, \tag{8b}$$

$$\lambda_{z,t} = \sqrt{\langle \langle w \rangle_z^2 \rangle_t - \langle \langle w \rangle_z \rangle_t^2}, \tag{8c}$$

$$\sigma_{t,z} = \left\langle \sqrt{\langle w^2 \rangle_t - \langle w \rangle_t^2} \right\rangle_z, \quad \text{and} \tag{8d}$$

$$\sigma_{z,t} = \left\langle \sqrt{\langle w^2 \rangle_z - \langle w \rangle_z^2} \right\rangle_t, \tag{8e}$$

where $\langle . \rangle_z = \int_{z_M}^{z_m} . \, dz/H$ and $\langle . \rangle_{t,z} = \int_{z_M}^{z_m} \langle . \rangle_t \, dz/H$; z_m and z_M are the minimum and maximum depth of the instrumented segment of the mooring, respectively; and $H = z_m - z_M$ is its vertical extent. The term μ defines the time- and vertical-mean value; $\lambda_{t,z}$ is the vertical standard deviation from the time mean; $\lambda_{z,t}$ is the temporal standard deviation from the vertical mean; $\sigma_{t,z}$ is the vertical

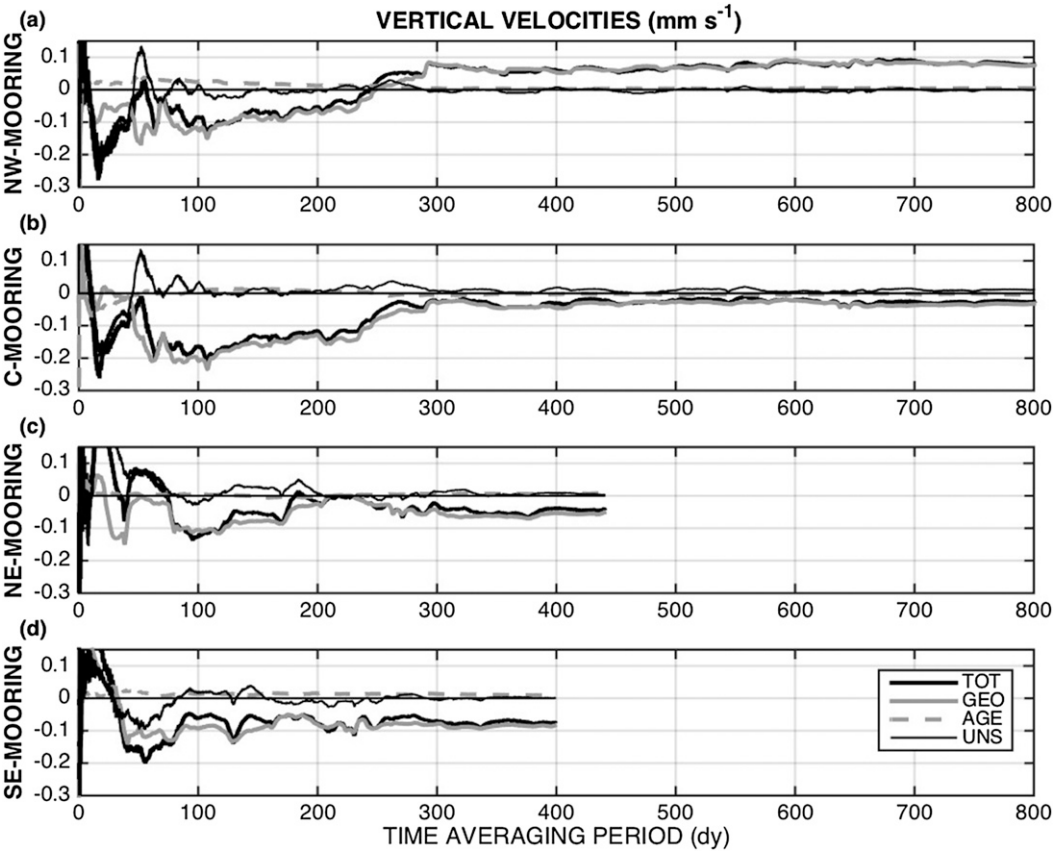

FIG. 5. Convergence of the time- and depth-averaged vertical velocity computed for each of the four moorings following (5): (a) NW, (b) C, (c) NE, and (d) SE. For each mooring, w is decomposed into its three components, following (6): w_g (thick solid gray), w_a (thick dashed gray), and w_u (thin solid black). The total vertical velocity is shown in thick solid black.

mean of the temporal standard deviation; and $\sigma_{z,t}$ is the temporal mean of the vertical standard deviation.

We also define a metric of the convergence of the vertical velocity calculation:

$$\mu_\tau = \frac{1}{\tau}\int_{t_i}^{t_i+\tau} \langle w \rangle_z \, dt, \tag{9}$$

where τ is the period of integration (between 0 and T). This diagnostic can be applied to both the total vertical velocity w or any of its individual components (w_g, w_a, and w_u).

c. Circulation setting of the measurements

As will be seen in section 4, the nature of the time-mean horizontal flow is important in controlling vertical motion across the DIMES mooring area. Specifically, the circulation in the deeper layers may be interpreted by considering theoretical work on stratified Taylor columns (Hogg 1973). We follow the work of Huppert (1975), who investigated the characteristics and vertical scale of a Taylor column over a topographic obstacle (akin to that encompassed by the DIMES mooring array) in a stratified flow. Using the same diagnostics as Meredith et al. (2003), we characterize the flow through the array by estimating the Burger number as $\mathrm{Bu} = -\langle N \rangle_{t,z} h/fL \simeq 4.6$ (where $h = 4400$ m is the ocean depth around the topographic obstacle, $L = 10$ km is the horizontal length scale of the topographic obstacle, and $\langle N \rangle_{t,z} = 1.7 \times 10^{-6}\,\mathrm{s}^{-1}$), the Rossby number as $\mathrm{Ro} = -\langle R \rangle_{t,z}/fL \simeq 0.1$ (with $\langle R \rangle_{t,z} = 0.12\,\mathrm{m\,s}^{-1}$), and the relative vertical length scale of the obstacle as $h_0 = |h'|/h \simeq 0.2$ (where $h' = -900$ m is the height of the topographic obstacle). This analysis yields $h_0/\mathrm{Ro} \simeq 2.1$, where h_0/Ro is a nondimensional critical height. For our diagnosed Burger number and nondimensional critical height, Huppert (1975) predicts the existence of a stratified Taylor column, thereby suggesting that the stratified Taylor column dynamics apply to our study area. This implies that close to the topographic obstacle, the circulating fluid is primarily guided by rotation (as opposed to stratification) and acts to conserve its potential vorticity. Also following Huppert (1975), we

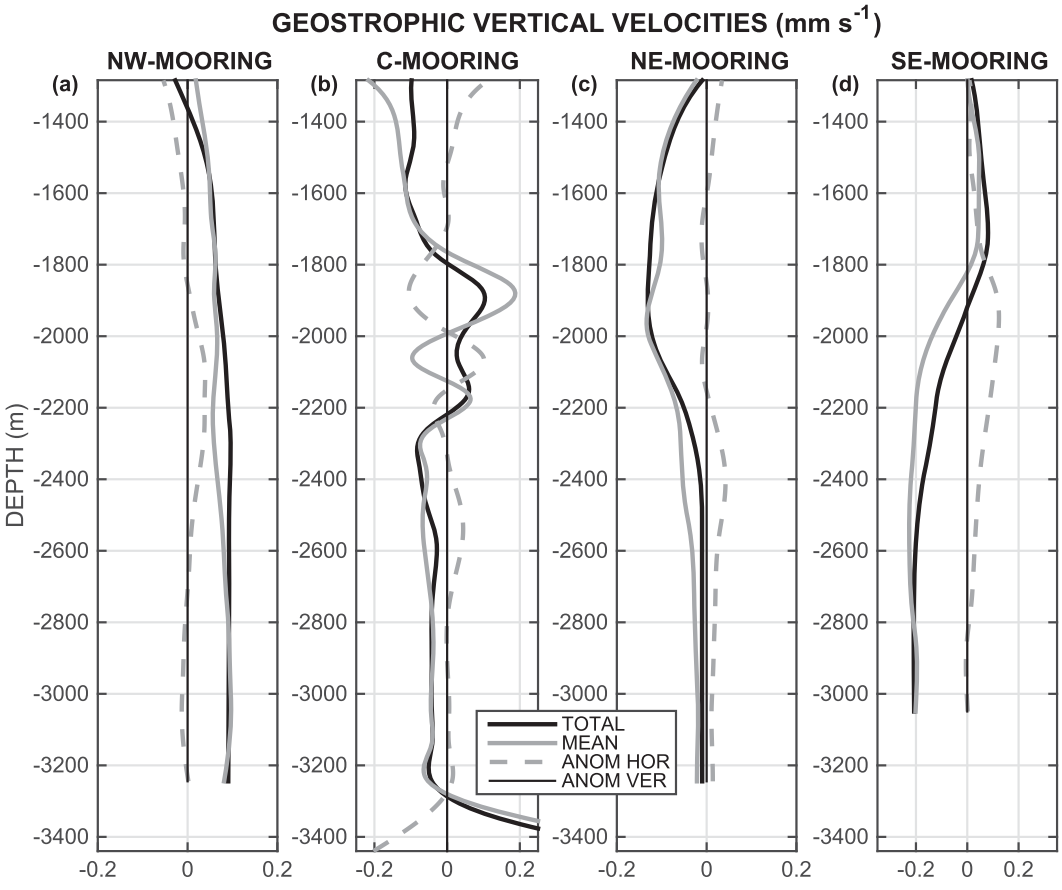

FIG. 6. Time-mean w_g computed for each of the four moorings following (6a): (a) NW, (b) C, (c) NE, and (d) SE. For each mooring, w_g is decomposed into its three components, following (7): the time-mean horizontal advection (thick solid gray), the anomalous horizontal advection (thick dashed gray), and the anomalous vertical advection (thin solid black). The term w_g is shown in thick solid black.

may estimate the Taylor column effect to have an e-folding decay height of $h_d = -f/\langle N\rangle_{t,z} L \simeq 60$ m. Thus, the Taylor column (rotation over the topographic obstacle) effect is expected to be significant up to a depth of $h + h' - h_d \simeq 2500$ m.

Consistent with this theoretical prediction, we observe that the time-mean horizontal flow is directed northeastward above 2500 m for all the moorings in the DIMES array (Fig. 2). Below 2500 m, however, the NW mooring exhibits southeastward flow, whereas the SE and NE moorings are characterized by north-northeastward flow. Thus, the circulation below 2500 m rotates anticlockwise as it passes over the topographic obstacle (Fig. 1). This implies an increase of (negative) relative vorticity over the topographic feature, as may be expected from the conservation of potential vorticity following the flow. Since the effects of rotation dominate over those of stratification only close to the topographic obstacle, this dynamical adjustment process, which is consistent with our set of (2) and its next order balance (Pedlosky 1979), is restricted to the abyssal ocean by the deep stratification (Brechner Owens and Hogg 1980). The extent to which the vertical velocity diagnosed from (5) to (7) is consistent with this theoretical expectation is assessed in the next section.

4. Results

Time-mean vertical velocities are dissimilar between the four moorings analyzed here (Table 2), despite the fact that the moorings are spaced at horizontal distances shorter than one first baroclinic Rossby deformation radius (approximately 15–20 km in the study area). For all four moorings, time-mean vertical velocities are dominated by the geostrophic term (Fig. 3). These time averages are a small residual of highly variable vertical velocities (Fig. 4; Table 2), as evidenced by the several order of magnitude gap between the time-mean vertical velocities and their standard deviation (at all depths and for all vertical velocity

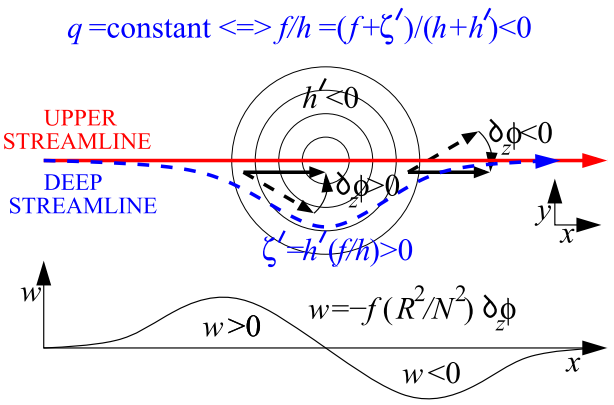

FIG. 7. Schematic of the flow over a small (horizontal length scale less than one first baroclinic Rossby radius) topographic obstacle, such as that encompassed by the DIMES moorings. A zonal flow (thick red solid and dashed blue lines in the upper and lower layers, respectively) over an obstacle of height h' (thin contours) deviates meridionally to conserve potential vorticity. In the Southern Hemisphere, this deviation induces a positive relative vorticity anomaly ($\zeta' = h'f/h > 0$, where h is depth above seabed) over the obstacle. With finite stratification, this Taylor column behavior is restricted to the deep ocean (Brechner Owens and Hogg 1980). This decouples the directions of horizontal flow in the upper and lower layers (thick solid and dashed arrows), leading to vertical motion w.

terms). Even for the geostrophic component, which shows the narrowest distribution (Fig. 4a), there is at least a one order of magnitude difference between the time mean and the standard deviation. These results stress the need for a time series of sufficient length to obtain accurate residuals.

Consistent with these results, in all moorings the geostrophic term dominates the time and depth mean μ, as well as the vertical structure of the time mean $\lambda_{t,z}$. By contrast, it is the unsteady term (related to $\partial_t\rho$) that dominates terms linked to time variation $\lambda_{z,t}$, $\sigma_{z,t}$, and $\sigma_{t,z}$ (i.e., the temporal variation of the vertical mean, the temporal mean of the vertical variation, and the vertical mean of the temporal variation, respectively).

The convergence diagnostic of (9) suggests that the temporal mean of the vertical velocity, which is mainly controlled by the geostrophic term, converges for averaging intervals of ~1 yr or longer (Fig. 5). This relatively long convergence is related to the cumulative effect of positive and negative eddylike events of intense vertical velocities ($\sim 5 \times 10^{-3}$ m s^{-1}; see Table 2 and Fig. 4) with a characteristic time scale of ~1 week, leading to a weak residual vertical velocity ($\sim 10^{-4}$ m s^{-1}; see Table 2 and Fig. 3) after approximately 1 yr. Further, since time-mean vertical velocities are residuals of highly variable features, convergence can be used to demonstrate the accuracy of the method. The convergence diagnostic thus allows us to quantify the uncertainty in time-mean vertical velocity. With fewer than 100 days of measurements, the variability of the time average is large, and so any conclusions on the time-mean vertical velocity are highly uncertain. Since our time series are substantially longer than 100 days, our vertical velocity estimates are robust. Note, however, that results from the SE and NE moorings should be considered with some caution, since they are based on data collected over only ~400 days.

To gain insight into how the mean vertical velocity is controlled by the geostrophic flow, we use (7) to decompose w_g. This decomposition reveals that time-mean geostrophic vertical motion is primarily shaped by the properties of the time-mean (rather than time varying) horizontal circulation (Fig. 6). This result suggests that the time-mean vertical flow in the study area is controlled by stationary features of the circulation and not by the transient eddy field (e.g., the cumulative nonlinear effects of successive mesoscale eddies or Rossby waves propagating through the mooring array).

Our study also reveals a peculiar property of the vertical velocity around 2500 m. Following the expectation set in section 3c, the horizontal stationary flow is modified in the deepest layers of the study area by the presence of a topographic obstacle, which leads to the occurrence of stratified Taylor column flow. Thus, below 2500 m, the horizontal stationary flow is deflected southward upstream of the topographic obstacle and northward downstream of it (Fig. 2). Following (6a), the change in the direction of horizontal flow between the layer above 2500 m (which is not influenced by the topographic feature) and that below 2500 m (which acts as a Taylor column) leads to vertical motion. Depending on whether the mooring is upstream or downstream of the topographic feature, this leads to an upward or a downward flow, respectively, at 2500 m (Fig. 7). We thus conclude that the deep vertical flow and its intricate spatial structure (i.e., upwelling at the NW mooring vs downwelling at the SE and NE moorings; Figs. 3, 6) are controlled by the presence of a deep, stationary, topographically locked meander or eddy structure in the horizontal flow of the ACC through northern Drake Passage.

5. Conclusions

Our main finding is that the time-mean vertical motion in the area of Drake Passage encompassed by the DIMES mooring cluster is primarily determined by the spatial structure of the time-mean geostrophic flow, which is linked to the underlying topography by stratified Taylor column dynamics. As the generally northeastward ACC flow passes over a topographic obstacle with lateral dimensions smaller than the first baroclinic

radius of deformation, upwelling (downwelling) occurs on the upstream (downstream) flank of the feature. This occurs as the deep-water column is compressed (stretched) and the deep horizontal flow acquires anticyclonic vorticity over the obstacle to conserve potential vorticity. A secondary result of our work is that the temporal variability in vertical velocity in the study region is largely associated with localized temporal variations in density.

Our diagnostic of vertical velocity is founded on the assumption of a small Rossby number. While we cannot prove that this assumption holds for all classes of flow exerting a significant influence on the mooring measurements, we may at least show that the results are not inconsistent with this assumption. Thus, calculating the vertical Rossby number for the horizontal momentum equations, that is, $(w\partial_z u)/(fv)$ and $(w\partial_z v)/(fu)$, reveals that for more than 75% of the mooring records Ro is smaller than 0.1, thereby lending support to the small Rossby number assumption.

Finally, this deep vertical motion associated with a sub-eddy-scale topographic obstacle stands in distinction to the common paradigm of large-scale Southern Ocean overturning linked to wind-driven Ekman and mesoscale eddy flows (Rintoul and Naveira Garabato 2013). While the wide gap in scales makes it very difficult to connect our results to the large-scale vertical circulation, it is worth noting that (unlike in an idealized, perfectly adiabatic Taylor column regime) the vertical flow over the topographic feature in our study area leads to a net vertical mass transport. This is because the stratification on the downstream (eastern) flank of the obstacle is different from that over the obstacle's upstream edge (Fig. 2). This difference may be due to enhanced diapycnal mixing at one flank of the obstacle (Dewey et al. 2005). In particular, the upward and downward steady flows around the obstacle are compatible with the appearance of lee waves, which can be conducive to shear instabilities and hence vertical turbulent flow in the region (Brearley et al. 2013). Given that bathymetric features with dimensions akin to those of the obstacle encompassed by the DIMES moorings are common across regions of rough topography in the ACC, the possibility that the process discussed in this work contributes significantly to large-scale vertical motion in the Southern Ocean deserves further attention.

In this context, we plan to extend our study to other regions of the Southern Ocean where mooring data are available. In particular, we will further investigate the relationship between stratified Taylor column and vertical velocities to develop a quantitative theoretical framework. In the longer term, extending this analysis to other mooring datasets beyond the Southern Ocean will allow us to test the spatial variation of the vertical motion on a more global scale. A particular focus will be to address the role of time-varying vertical velocities in ocean circulation.

Acknowledgments. This research was supported by the U.K. Natural and Environmental Research Council (MESO-CLIP Grant NE/K005928/1 and DIMES Grant NE/F020252/1). We thank the editor, Herlé Mercier, and two anonymous reviewers for their useful comments that improved the manuscript.

REFERENCES

Abernathey, R., J. Marshall, and D. Ferreira, 2011: The dependence of Southern Ocean meridional overturning on wind stress. *J. Phys. Oceanogr.,* **41,** 2261–2278, doi:10.1175/JPO-D-11-023.1.

Brearley, J. A., K. L. Sheen, A. C. Naveira Garabato, D. A. Smeed, and S. Waterman, 2013: Eddy-induced modulation of turbulent dissipation over rough topography in the Southern Ocean. *J. Phys. Oceanogr.,* **43,** 2288–2308, doi:10.1175/JPO-D-12-0222.1.

Brechner Owens, W., and N. G. Hogg, 1980: Oceanic observations of stratified Taylor columns near a bump. *Deep-Sea Res.,* **27,** 1029–1045, doi:10.1016/0198-0149(80)90063-1.

Bryden, H. L., 1980: Geostrophic vorticity balance in mid-ocean. *J. Geophys. Res.,* **85,** 2825–2828, doi:10.1029/JC085iC05p02825.

Cronin, M., K. L. Tracey, and D. R. Watts, 1992: Mooring motion correction of SYNOP central array current meter data. University of Rhode Island Tech. Rep. 92-4, 114 pp.

Cushman-Roisin, B., and J.-M. Beckers, 2011: *Introduction to Geophysical Fluid Dynamics: Physical and Numerical Aspects.* Academic Press, 875 pp.

D'Asaro, E. A., R.-C. Lien, and F. Henyey, 2007: High-frequency internal waves on the Oregon continental shelf. *J. Phys. Oceanogr.,* **37,** 1956–1967, doi:10.1175/JPO3096.1.

Dewey, R., D. Richmond, and C. Garrett, 2005: Stratified tidal flow over a bump. *J. Phys. Oceanogr.,* **35,** 1911–1927, doi:10.1175/JPO2799.1.

Farneti, R., and T. L. Delworth, 2010: The role of mesoscale eddies in the remote oceanic response to altered Southern Hemisphere winds. *J. Phys. Oceanogr.,* **40,** 2348–2354, doi:10.1175/2010JPO4480.1.

Garrett, C., P. MacCready, and P. Rhines, 1993: Boundary mixing and arrested Ekman layers: Rotating stratified flow near sloping boundary. *Annu. Rev. Fluid Mech.,* **25,** 291–323, doi:10.1146/annurev.fl.25.010193.001451.

Gill, A. E., 1982: *Atmosphere–Ocean Dynamics.* Academic Press, 662 pp.

Hallberg, R., and A. Gnanadesikan, 2006: The role of eddies in determining the structure and response of the wind-driven Southern Hemisphere overturning: Results from the Modeling Eddies in the Southern Ocean (MESO) project. *J. Phys. Oceanogr.,* **36,** 2232–2252, doi:10.1175/JPO2980.1.

Hogg, N. G., 1973: On the stratified Taylor column. *J. Fluid Mech.,* **58,** 517–537, doi:10.1017/S0022112073002302.

Holton, J. R., 1972: *An Introduction to Dynamic Meteorology.* Academic Press, 319 pp.

Huppert, H. E., 1975: Some remarks on the initiation of Taylor columns. *J. Fluid Mech.,* **67,** 397–412, doi:10.1017/S0022112075000377.

Krauss, W., 1966: *Interne Wellen.* Borntraeger, 248 pp.

Manucharyan, G., W. Moon, F. Sévellec, A. J. Wells, J.-Q. Zhong, and J. S. Wettlaufer, 2014: Steady turbulent density currents on a slope in a rotating fluid. *J. Fluid Mech.,* **746,** 405–436, doi:10.1017/jfm.2014.119.

Marshall, J., and K. Speer, 2012: Closure of the meridional overturning circulation through Southern Ocean upwelling. *Nat. Geosci.,* **5,** 171–180, doi:10.1038/ngeo1391.

McDougall, T. J., and P. M. Barker, 2011: Getting started with TEOS-10 and the Gibbs Seawater (GSW) oceanographic toolbox. SCOR/IAPSO WG127, 28 pp. [Available online at www.teos-10.org/pubs/Getting_Started.pdf.]

Meredith, M. P., 2011: Cruise report, RRS James Cook JC054 (DIMES UK2): 30 November 2010 to 8 January 2011. British Antarctic Survey Cruise Tech. Rep., 206 pp.

——, and Coauthors, 2003: An anticyclonic circulation above the Northwest Georgia Rise, Southern Ocean. *Geophys. Res. Lett.,* **30,** 2061, doi:10.1029/2003GL018039.

Naveira Garabato, A. C., 2010: RRS James Cook cruise 041: 05-21 Dec 2009. National Oceanography Centre Southampton Cruise Rep. 56, 164 pp.

Olbers, D., D. Borowski, C. Völker, and J.-O. Wölff, 2004: The dynamical balance, transport and circulation of the Antarctic Circumpolar Current. *Antarct. Sci.,* **16,** 439–470, doi:10.1017/S0954102004002251.

Osborne, A. R., and T. L. Burch, 1980: Internal solitons in the Andaman Sea. *Science,* **208,** 451–460, doi:10.1126/science.208.4443.451.

Pedlosky, J., 1979: *Geophysical Fluid Dynamics.* Springer-Verlag, 624 pp.

Polzin, K. L., J. M. Toole, J. R. Ledwell, and R. W. Schmitt, 1997: Spatial variability of turbulent mixing in the abyssal ocean. *Science,* **276,** 93–96, doi:10.1126/science.276.5309.93.

Rintoul, S. R., and A. C. Naveira Garabato, 2013: Dynamics of the Southern Ocean circulation. *Ocean Circulation and Climate: A 21st Century Perspective,* G. Siedler et al., Eds., International Geophysics Series, Vol. 103, Academic Press, 471–492.

Sérazin, G., 2011: An approximate neutral density variable of the world's oceans. M.Sc. Thesis, École Centrale Lyon, 85 pp.

Sheen, K. L., and Coauthors, 2013: Rates and mechanisms of turbulent dissipation and mixing in the Southern Ocean: Results from the Diapycnal and Isopycnal Mixing Experiment in the Southern Ocean (DIMES). *J. Geophys. Res. Oceans,* **118,** 2774–2792, doi:10.1002/jgrc.20217.

van Aken, H. M., H. van Haren, and L. R. M. Maas, 2007: The high-resolution vertical structure of internal tides and near-inertial waves measured with an ADCP over the continental slope in the Bay of Biscay. *Deep-Sea Res. I,* **54,** 533–556, doi:10.1016/j.dsr.2007.01.003.

Waterman, S., A. C. Naveira Garabato, and K. L. Polzin, 2013: Internal waves and turbulence in the Antarctic Circumpolar Current. *J. Phys. Oceanogr.,* **43,** 259–282, doi:10.1175/JPO-D-11-0194.1.